Connecting fluvial levee deposition to flood-basin hydrology

Authors: Graham H. Johnston[1], Scott R. David[1,2], and Douglas A. Edmonds[1*]
(1) Department of Earth and Atmospheric Sciences, Indiana University
(2) Department of Geosciences, University of Massachusetts Amherst
*corresponding author, edmondsd@indiana.edu

Key Points:

1. Empirical analyses of lidar data show that levee size and shape on the Muscatatuck River, IN are unrelated to the channel planform.
2. Numerical modeling reveals that levees are unrelated to the channel planform because their growth is dictated by inundation dynamics in the floodbasin
3. On tall levees, the levee toe grows faster than the levee crest because it is inundated more frequently, and this causes levees to prograde down-valley over time.

Abstract

Levees are commonly found along every kind of river system, yet there are no widely accepted models for where along the channel they form and what controls their shape. In this study, we investigated whether levee growth is driven by sediment transfer from the channel adjacent to the levee or by inundation dynamics in the flood-basin. To test these ideas, we conducted empirical analyses and numerical modeling of levees on the fine-grained, meandering Muscatatuck River, IN. Using lidar data, we found no statistical relationship between the levee and the adjacent channel planform, which suggests levees are not genetically related to their adjacent channel. Surprisingly, modeling experiments of a simplified Muscatatuck River show that levee initiation can be genetically related to the adjacent channel because bed shear stress on the floodplain is low where channel curvature is high. But after levees initiate, the genetic connection to the adjacent channel is obscured because their shape is modified by inundation dynamics. Tall, mature levees are not inundated regularly and instead obstruct floodplain flow, creating flow shadows on the downstream side. Sediment is preferentially deposited in the flow shadow, which moves the location of maximum

deposition from the levee crest to the toe. This causes levees to prograde down-valley, which in turn reshapes the levee and genetically disconnects it from the channel. We propose that this morphodynamic mechanism of levee growth is characteristic of fine-grained rivers where flood-basins can act as conveyance channels that transport sediment downvalley before deposition.

1. Introduction

Fluvial levees are important geomorphic features located along the banks of alluvial rivers. Levees dictate flooding patterns, and the bi-directional exchange of water, sediment, and pollutants between the channel and floodplain [*Nanson and Croke*, 1992; *Brierley et al.*, 1997; *Adams et al.*, 2004]. This, in turn, affects soil development, agricultural activity, and hazards to population centers within the flood basin [*Wolfert et al.*, 2002; *Brakenridge et al.*, 2017]. Levees also influence fluvial stratigraphy because as they grow, the potential for avulsion increases as the water surface becomes elevated above the floodplain [*Bryant et al.*, 1995; *Mackey and Bridge*, 1995; *Mohrig et al.*, 2000]. Due to their stratigraphic architecture, levee deposits are often targeted for hydrocarbons [*Fielding and Crane*, 1987]. Despite the societal and scientific importance of levees we do not know what sets their presence, size, and shape.

Our current understanding of levee deposition is surprisingly cursory—empirical studies thus far have not revealed consistent controls on levee presence, size, or shape. Levees are thought to occur along both banks of a river, but on some meandering rivers they are more pronounced along the cut-bank where they are not disturbed by scroll bar formation [*Kesel et al.*, 1974; *Hudson and Heitmuller*, 2003; *Brooks*, 2005]. However in other cases, levees show little preference and occur on most river banks [*Smith et al.*, 1989], only on straight reaches [*Ferguson and Brierley*, 1999], or on alternating sides [*Iseya and Ikeda*, 1989]. Levee shape should also be related to the sediment load, because all else being equal, channels with fine-grained sediment should produce wide levees, with gentle slopes as sediment

is transferred farther into the floodplain, whereas channels with coarser-grains should have narrow, steep levees. Indeed, this occurs in some fluvial systems [*Cazanacli and Smith*, 1998; *Hudson and Heitmuller*, 2003], but in many cases, fine-grained levees can be steeper than coarse-grained ones [*Ferguson and Brierley*, 1999] and the relationship between grain size and levee shape is often ambiguous [*Adams et al.*, 2004]. These empirical studies show no consistent results because we still do not know the basic conditions for levee formation making it hard to isolate controls on levee shape.

Levees form when sediment is deposited in a zone of reduced flow competence along the channel margins. A reasonable starting assumption is that the levee is genetically related to the adjacent channel and thus the local channel and sediment characteristics—planform, depth, width, hydrology, and grain settling—govern movement of sediment to the margins where levees form. This notion is encapsulated in early models: assuming a straight channel, it can be shown that suspended sediment is transferred to the channel margin by fluid advection and turbulent eddy diffusion [*James*, 1985; *Pizzuto*, 1987; *Shiono and Knight*, 1991; *Marriott*, 1992; *Nezu and Nakagawa*, 1993; *Mertes*, 1997; *Adams et al.*, 2004; *Pizzuto et al.*, 2008]. These studies promote the idea that the levee is genetically related to the adjacent channel segment, even though field data are equivocal and show no consistent relationship between the levee and any measure of the adjacent channel.

On the other hand, levees may not be genetically related to the adjacent channel, especially if levee sediment originates from sediment-laden floodwaters moving down-valley. This implies that flood basins are more than just water storage locations—they convey water and sediment long distances, sculpting levees in the process [*Filgueira-Rivera et al.*, 2007; *Pierik et al.*, 2017]. For instance, floodplain sedimentation patterns are sensitive to floodplain microtopography, inundation time, flood wave shape, flood magnitude, and the presence of perirheic zones [*Asselman and Middelkoop*, 1995; *Mertes*, 1997; *Middelkoop and Van der Perk*, 1998; *Walling and He*, 1998; *Nicholas and Mitchell*, 2003; *David et al.*, 2017]. One interesting example shows that levee deposition occurs even when water in the adjacent

channel does not overtop the levee. *Filgueira-Rivera et al.* [2007] demonstrate that the levee crest and toe can grow quasi-independently because the toe is at a lower elevation and is inundated by sediment-laden water more frequently. This suggests levee deposition may not be related to the adjacent channel, but instead occurs as the flood wave transports fine-grained sediment down-valley to positions behind fluvial levees on the floodplain. The ultimate levee form may be dictated by flood-basin hydrology and sediment transport during flood rather than the detailed mechanisms of sediment transfer from the adjacent channel to the margin.

The focus of this paper is to assess whether levee presence and geometry are genetically related to the adjacent channel or to flood-basin hydrology. We assess this by measuring and modeling levee presence, size and shape on the meandering Muscatatuck River, Indiana. We have two hypotheses for how levee deposition should be connected to the adjacent channel in meandering rivers. Our first hypothesis is that levee heights and widths should scale with curvature because curvature drives superelevation of the water surface and promotes advective sediment transport across cutbanks [*Ervine et al.*, 1993; *Ervine et al.*, 2000]. Our second hypothesis is that levees should be most prevalent and largest in the crossover region (i.e. where the channel centerline is perpendicular to the floodplain centerline) because this is where advective transport of channel sediment into the floodplain is maximized [*Shiono and Muto*, 1998; *Ervine et al.*, 2000; *Czuba et al.*, accepted]. Our alternative hypothesis is that levee formation is not related to the adjacent channel, and instead dictated by flood-basin hydrology. To test these hypotheses, we conducted an empirical analysis of near channel topography along the Muscatatuck River, IN and its association with the adjacent channel curvature and orientation relative to floodplain centerline. We assess the role of the floodbasin with numerical modeling. Based on our numerical modeling, we show how levee deposition can occur independently of the adjacent channel and how levee form in this scenario is ultimately governed by floodbasin hydrology.

2. Field Study Site

Our field study focuses on the Muscatatuck River (Figure 1), which flows westward from the Muscatatuck Plateau across the Scottsburg Lowlands through southern Indiana eventually meeting the East Fork White River to the west. The Scottsburg Lowlands run approximately north-south between the Muscatatuck Plateau to the east and the Norman Upland to the west. This region lies south of the Wisconsin Glaciation boundary and may have served as a conduit for glacial outwash flowing south to the Ohio River. Underlying this physiographic region is Devonian and Mississippian age limestone, shale and siltstone. Across this area, the Muscatatuck River continues to incise into sediments weathered from the underlying New Albany Shale to the east and the Borden Group shales to the west. The Muscatatuck River incision into this easily eroded, fine-grained siltstone and shale accounts for the fine-grained sediment load.

We selected two reaches along the Muscatatuck River for detailed analysis of the near-channel topography (Figure 1A, B). We refer to the topography as near-channel because not all reaches contain levees. These reaches were chosen because both are prone to frequent flood events that fully inundate the surrounding floodplains, and both have levees along the channel margins. Also, neither of the reaches are lined with anthropogenic flood control structures, such as dikes or dams, or elevated road beds which would obscure natural features. Both reaches flow through low gradient, agricultural land in southern Indiana.

We analyzed near-channel topography using a 1.5-meter resolution, bare earth digital elevation model (DEM), derived from LiDAR data accessed at opentoography.org. The LiDAR dataset was collected by a nonprofit consortium during the statewide campaign to collect high resolution LiDAR and orthophotography data from 2011 to 2013. Reach 1 has a channel centerline distance of 5,210 meters, the average channel width is 28 meters, and the sinuosity—measured as the channel centerline distance divided by the upstream to downstream straight-line distance—is 1.78 (Figure 1A). Reach 2 is located

approximately 8.9 km downstream from Reach 1 and has a channel centerline distance of 7,557 meters, the average channel width is approximately 32 meters, and the sinuosity is 3.04 (Figure 1B). The floodplain slopes for Reach 1 and Reach 2 are 0.00033 and 0.00027, respectively; and the channel bed slopes for Reach 1 and Reach 2 are 0.00021 and 0.00011, respectively. The average bankfull depth through both reaches of the Muscatatuck measured from a single-beam echo sounder is approximately 2-meters.

To characterize the suspended sediment concentrations in the Muscatatuck River we collected 51 suspended sediment samples and augmented these data with 92 suspended sediment concentration samples collected by the USGS at the stream gage in Deputy, Indiana (Figure 1C). We collected suspended sediment samples from four bridges spanning the Muscatatuck River (denoted by stars in Figure 1C) on February 7, 2015; March 4 and 11, 2015; April 12, 2015 and January 21, 2017 during bankfull to flood stage discharge (20 – 198 m^3/s) according to USGS standard operating procedures using a US-DH59 sampler [*Edwards et al.*, 1999]. Suspended sediment concentrations were measured with the evaporation method procedures laid out in the ASTM International Test Method, D 3977 – 97(B).

To characterize the grain-size in the channel and floodplain, we collected four channel-bed-surface sediment samples during bankfull to floodstage flow, and ten hand auger samples from the levee and ten from the floodplain. Channel-bed-surface samples were collected from the Waskom and Wheeler Hollow bridges (Figure 1C) on January 20, 2016 using a Ponar® grab sampler according to standard operating procedures laid out by the U.S. Environmental Protection Agency in SESDPROC-200-R3. Levee and floodplain deposits were sampled at Reach 2 using a hand auger (Figure 1D). Two replicate samples were collected at each location, and samples for analysis were taken 0.75 meters below the surface to avoid sampling organic root material or surface soil that may have been modified by agricultural activities. Grain size was measured with a Malvern Mastersizer® 3000E.

149 The Muscatatuck River is silt-dominated with moderate to high suspended sediment concentrations.
150 Combining our samples and ones from USGS, the average suspended sediment concentration during
151 bankfull flow (Q = 35 m^3/s) or higher for the Muscatatuck River is 0.23 kg/m^3 (Figure 2A). The median
152 grain size for suspended and bed-surface sediment was 15.7 µm and 27.7 µm, respectively. Median
153 grain size for the levee and floodplain deposits were 9.8 µm and 10.1 µm, respectively (Figure 2B). There
154 was no systematic difference in the channel-bed grain size across the four measurement locations.
155
156 # 3. Methods

157 *3.1 Measuring Near-channel Topography*

158 Measuring near channel topography is a deceptively challenging task. Idealized levee shapes are
159 conceptually simple—most models depict levees as gull-wing shaped deposits with elevations that
160 exponentially taper from a maximum at the crest out to the levee toe [*Hudson and Heitmuller*, 2003].
161 But natural levees rarely follow this shape and instead show a wide variability of shape and orientation
162 relative to the channel margin. This variability and complexity is not captured when levee geometry is
163 measured with coarsely-spaced cross-sections perpendicular to the channel centerline.
164 The methodology we have developed captures the full two-dimensional planform shape of the
165 levee. We first detrend the DEM by removing the average floodplain slope from the topography. The
166 average floodplain slope was derived from a triangulated irregular network (TIN). The TIN surface was
167 computed by sampling elevations along evenly spaced cross-sections down the floodplain. The resulting
168 TIN surface maintained all long wavelength topography and removed all short wavelength topography.
169 We found that using this surface to remove down-valley slope minimized distortion of small scale
170 features when detrending the floodplain. Next, we isolate near channel topography in the LiDAR data
171 within three channel widths along both banks using a histogram equalization method. This method is
172 often used by the medical industry to analyze x-rays because the data distribution is reshaped to create

a linear cumulative distribution function, which has the distinct advantage of enhancing low contrast areas [*Hum et al.*, 2014]. In the context of a DEM, this enhances the low relief of the levee toe where slopes are small (Figure 3).

Using the histogram equalized image, we then pick an elevation value for the levee toe by inspecting cross-sections. Like previous researchers, we identify the levee toe on different cross-sections as the location where the levee slope decreases to approximately 0.01 m/m [*Cazanacli and Smith*, 1998; *Filgueira-Rivera et al.*, 2007]. In areas where levee deposits abut more complex topographic surfaces we determined the levee toe by defining the first major break in topography after the levee crest [*Adams et al.* [2004]. Otherwise, the levee toe was delineated from changes in land use or vegetation [*Hudson and Heitmuller, 2003*]. The levee toe contour elevation was determined by thorough inspection of individual cross-sections and analysis of satellite and hillshade imagery. We avoided any anthropogenic features, such as elevated road beds or drainage ditches. Additionally, natural features not genetically related to the channel, such as fluvial terraces and continuous low angle hillslopes, were excluded from the levee analysis (inset A, Figure 3).

We then define individual levee polygons from closed contours at the elevation of the levee toe (Figure 4). Closed contours define a single levee, and in some cases, these are generated by depositional processes, whereas in other cases channels cut through the levees (inset B, Figure 3). Levee width for each polygon was calculated by calculating channel-perpendicular transects, spaced 2-meters apart, and clipping them at levee polygon boundaries (Figure 4, inset). Average levee width is calculated as an arithmetic mean of all cross-sections within a given polygon on each channel bank. Levee height values were extracted as the highest value for each channel-perpendicular transects and then averaged across all transects. Local channel centerline curvature was measured using RivMAP [*Schwenk et al.*, 2017]. We also calculate the radius of curvature by fitting a circular arc to the channel centerline using satellite

196 imagery available through Google Earth Pro®. The channel centerline was defined as the mid-point
197 between the cutbank and the inside point bar.

198 Finally, we calculated the orientation of levee deposits relative to the floodplain centerline. The
199 levee and floodplain centerlines were determined with Thiessen polygons. We grow the Thiessen
200 polygons from the boundaries of the levee and floodplain polygons. The levee polygons were defined by
201 the levee toe contours, and the floodplain polygon was defined by floodplain terrace boundaries. The
202 line where the Thiessen polygons meet is taken as the levee and floodplain centerlines. The angle
203 between the two centerlines was measured as the difference between the azimuth orientation of each
204 centerline measured in degrees.

205

206 *3.2 Numerical Modeling Methods*

207 3.2.1 Flow modeling considerations in Delft3D

208 We conducted numerical modeling experiments using Delft3D, which solves the coupled 3D fluid
209 flow field and bed evolution. For 3D flow, Delft3D solves the shallow-water equations with a user
210 specified number of depth layers. In this paper we used eight layers with thicknesses (as a percentage of
211 total depth) moving from the water surface to the bed as 30, 20, 10, 10, 10, 10, 5, and 5%. The vertical
212 transport of momentum between the flow layers is accounted for using the κ-ε turbulence closure
213 model which solves for the kinetic energy (κ) and the turbulent kinetic dissipation (ε). These values are
214 used to determine the vertical eddy viscosity and the mixing length of the flow. In addition to the
215 transport of fluid momentum, Delft3D models the transport of suspended sediment by solving the
216 conservation of mass of suspended material within the model domain. The model solves for the 3D
217 transport of sediment by calculating the advection and diffusion of suspended particles using the flow
218 velocity terms and the eddy diffusivities derived using the Navier-Stokes equations.

219 3.2.2 Model Domain Selection

To explore controls on levee depositional patterns, we choose a model domain covering a channel reach with several meander bends that allowed for an examination of the hydrodynamic conditions during flood events. We selected Reach 2 for this analysis (Figure 1B) because it contains multiple river meander bends and we know that levees have formed along the channel. The modeling domain covers a floodplain area that is 2,500 meters long by 1,700 meters wide. Our model domain is the same extent as shown in Figure1B. In the model we retain the shape of the river in planform, but synthetically flattened the floodplain topography so we could easily assess how the flood-wave interacts with the channel during flood. The smoothed floodplain has a slope of ~0.00027 m/m and channel slope of ~0.00011 m/m, consistent with field observations. The channel was 2-meters deep, consistent with field measurements, and with a rectangular cross-sectional shape. A random centimeter-scale topographic perturbation was also added across the model domain to the surface to allow for more realistic flow propagation. We added a straight channel segment at the upstream boundary of the model for flow establishment prior to entering the first meander bend. We also smoothed the channel bankline boundaries to encourage a more natural flow condition and eliminated grid effects.

3.2.3 Boundary Conditions and Physical Parameters

Flow direction enters the domain along the eastern boundary and exits to the west. The upstream boundary was set across the channel width at the eastern boundary and defined the time-dependent fluid discharge entering the domain. The downstream boundary was a time-varying water level elevation that was chosen to prevent backwater or drawdown effects based on the upstream discharge. The north and south model boundaries were defined as Neumann boundaries, which allows fluid and sediment to smoothly exit or enter the boundary. At the upstream boundary, the incoming sediment flux was set to a constant 0.23 kg/m^3 with a density of 2,650 kg/m^3, and a grain size of 0.016 mm. This size was determined based on the median grain size of suspended sediment sampled during field

operations. The settling rate of grains is 0.23 mm/s [*Ferguson and Church*, 2004]. Additional modeling parameters are summarized in Table 1.

The primary factors that drive suspended sediment deposition and erosion within the modeling domain are the critical shear stress for sedimentation and erosion. There are numerous factors, such as vegetation, microtopographic variations, grain flocculation, for example, that cause deposition of silt and clay sized grains on the floodplain. Our model was not able to account for all of these factors. In order to allow for deposition of sediment during a flood event, we set the critical shear stress for sedimentation at 0.5 N/m^2. This value permits a reasonable amount of deposition in the domain. The critical shear stress for erosion is set to 2 N/m^2. This value falls within the reasonable range for erosive shear stresses for fine-grained, cohesive sediment and does not allow for excessive channel erosion during elevated discharge events [*Clark and Wynn*, 2007; *Kimiaghalam et al.*, 2016]. Based on historical satellite imagery, we know that the channels of the Muscatatuck are relatively stable, and any shear stress values for erosion that allow for rapid changes to the channel planform are not representative of the natural system. Deposition of fine-grained silt within the model domain occurs slowly, so we used a morphological scaling factor of 70 for these modeling experiments to speed up change.

3.2.4 Modeling Experiment and Sensitivity

To quantify the evolution of levee morphology, we flooded the model domain from the upstream boundary four times with identical triangular flood waves. The flood waves were symmetrical and peaked at 100 m^3/s. Each flood wave lasted two days and started and stopped at a minimum discharge of 10 m^3/s. The peak discharge completely inundated the floodplain, and floodplain waters exited the domain before the next flood event. The entire four wave experiment lasted eight days of model time. It is difficult to scale this time precisely, but the discharge magnitude roughly corresponds

to 0.5 to 1-year flood and given the morphological scale factor of 70, we argue these simulations could represent 140-280 years of actual time.

We assessed the model sensitivity by comparing flow conditions and depositional patterns while varying several physical parameters, the grid resolution, and boundary conditions. The model proved insensitive to implementation of the two-dimensional horizontal large eddy simulation available with the Delft3D modeling package. Model results were also insensitive to finer grid resolutions. Computation time increased dramatically when decreasing grid cell size from 10-meter by 10-meter to 5-meter by 5-meter, but the depositional patterns and hydrodynamic conditions were unchanged. Finally, variations in suspended sediment concentrations at the upstream boundary did not affect the planform depositional patterns. The volume of sediment deposited within the domain was affected by reductions in the sediment concentration, but the locations and lateral extent of deposits were unaffected.

Model results were sensitive to the horizontal eddy viscosity value, the type of boundary conditions along the northern and southern boundaries, and the threshold water depth. Increasing the eddy viscosity value by one and two orders of magnitude resulted in increasing grid effects to fluid flow across the model domain. High values of eddy viscosity limited diffusion of eddies flowing from one grid cell to another. Changing the northern and southern boundary conditions to closed boundaries resulted in different flood wave propagation and depositional patterns along the distal margins of the domain when compared to the results using neumann boundaries. Closed boundaries forced abrupt down-valley change in flow vector orientation and often modified the shape of the distal edge of sedimentation patterns. Lastly, variations in the water threshold depth, value for determining if a cell is wet or dry, caused unrealistic deposition across the domain. Elevated threshold values often caused grid cells with shallow water depths to fluctuate between wet and dry conditions during the initial inundation of the

floodplain and as waters receded during the falling limb of a flood wave. This resulted in unrealistic, gridded depositional patterns along the leading edge of the flood wave.

4. Controls on levee morphology on the Muscatatuck River

Based on our definition of levees and methods for their delineation, we mapped the presence of levees along the two reaches of the Muscatatuck River (Figure 5). On Reach 1 levees are more common and occur along 80% of the banks, whereas in Reach 2 levees occur along 55% and 10% of the left and right banks, respectively (Figure 5). River right and river left series show some degree of correspondence on both reaches. In Reach 1, both sides have a decreasing levee presence until normalized stream distance of 0.1 and then become progressively more leveed downstream. In Reach 2, both river right and left have unleveed portions from normalized stream distances of 0.5 to 0.75. This suggests that levees tend to be paired. For a given reach, paired levees show little similarity between their heights and widths at a given position (Figure 6). We find no statistical evidence that these series are correlated. Median levee heights and widths for both reaches are reported in Table 2.

To explore controls on levee shape, we compared the local channel centerline curvature for both reaches to levee geometry. We calculated the channel curvature as the second derivative of the channel centerline (Schwenk et al., 2017) (Figure 6C,F). We calculated the cross-correlation between the curvature series and levee width or height to see if levee geometry is in phase (plus or minus a lag) with channel planform. We found that levee morphology is not in phase with channel curvature (Figure 7). In some cases, there may be a slight correlation between levee width and channel curvature (e.g., river right levees along Reach 1 at the zero-lag position, Figure 7). But, the value does not rise significantly above the background. These results suggest that variations in the height and width of levees along the Muscatatuck River is unrelated to channel curvature.

For Reaches 1 and 2, we also explored whether levee morphology was determined by the orientation between levee centerline and floodplain centerline (Figure 8). Angle values near zero

degrees indicate a levee centerline runs approximately parallel with a floodplain centerline, and values approaching 90 degrees indicate a levee centerline is perpendicular to the floodplain centerline. There is no obvious relationship between the orientation of the levee relative to the floodplain and all levee variables considered (Figure 8).

We finally explored the relationships between channel radius of curvature and levee geometry for 54 meander bends along the Muscatatuck River. For this analysis, we increased our study reach to 44 kilometers of channel centerline distance to include more meander bends (Figure 1C). For these bends, we only considered cutbanks where levees are not obscured by scroll bars and easier to identify. We found no relationship between channel radius of curvature and levee morphology (Figure 8). That said, meander bends with the highest radius of curvature values are loosely associated with narrower and taller levees, however, this could be a sample size bias at larger radii of curvature (Figure 9A,B). Aspect ratio, and basal area showed a high degree of variability across the range of channel radius of curvature values and no clear relationships exist (Figure 9C,D).

In summary, these empirical data show no clear relationship between the adjacent channel and levee formation. We think this suggests that levee deposition on the Muscatatuck is instead governed by flood-basin hydrology and in the following section we test how a fine-grained river system creates levees during overbank flow.

5. Morphodynamic modeling of levee formation

To explore the processes that lead to levee formation and growth on the Muscatatuck River, we model levee morphodynamics in Delft3D along Reach 2 through four consecutive flood waves. Each flood wave is symmetrical and peaks at 100 m^3/s discharge and starts and stops at a minimum of 10 m^3/s discharge. Bankfull discharge is achieved at approximately 35 – 40 m^3/s. Peak discharge results in

complete inundation of the floodplain while still maintaining the high velocity channelized flow. Floodplain water depth during peak inundation is approximately 0.5 meters.

Prior to the morphodynamic simulation, we first simulated the reach with only hydrodynamics. In this case, as the flood wave moves down-valley, there is surprising variability in flood-wave arrival times given the simplicity of the floodplain (Figure 10A). For instance, the southern half of the floodplain inundates later than the northern half. This could be caused by the interaction of the flood with the meandering channel, which serves as a macro roughness element. During peak inundation, there are distinct zones of high and low bed shear stress that emerge as the flood wave interacts with the channel (Figure 10B). Downstream of meander bend apices, the expulsion of high velocity channel waters creates locally high bed shear stress [*Sellin et al.*, 1993; *Shiono and Muto*, 1998]. However, at the apex of the meander bend channel and floodplain flow are aligned and shear stress in this region low.

During the four flood waves, some sediment is deposited on the channel bed, but most of the deposition occurred along the channel margins and across the floodplain (Figure 11). Levee deposition occurs where the bed shear stress is less than the critical value for sedimentation (0.5 Pa, Table 1) in our experiments (compare Fig. 10B and 11). Interestingly, the thickest levee deposits occur at meander bend apices where channel curvature is highest. As expected, total levee deposit thicknesses are small; typically, on the order of 10 to 20 centimeters, but they are consistent with field measurements (Table 2; Figure 6).

Many areas across the modeling domain show interesting depositional patterns, but we focus on four areas that include three cutbank levee deposits (labeled 1 through 4 on Figure 11). Levees at locations 1 and 2 are oriented approximately 45 and 30 degrees, respectively, relative to the down-valley flow direction. Levees at location 3 and 4 are oriented approximately parallel to the down-valley slope. Temporal evolution of levee shape and size show that all levees grow down valley during subsequent flooding events (Figure 12). Down-valley progradation is especially evident for location 1

where levee growth is oblique to the channel bank at the meander bend apex. The levee at location 1 also widens as it grows in a down-valley direction. Levee 2 also undergoes widening and down-valley progradation. Progradation of the levee at location 3 is less pronounced; however, this deposit also widens and begins to grow in a down-valley direction after the second flood wave. Down-valley progradation is evident along the left bank at location 4, and both paired levees experience lateral widening.

Down-valley progradation occurs because when the levee grows it generates a morphodynamic feedback by shifting deposition from the crest to the toe [*Filgueira-Rivera et al.*, 2007]. All levees undergo a transition from crest to toe deposition by the fourth flood waves (Figure 12, 13). The change maps for each levee (Figure 12) show that deposition on the crest decreases from flood wave 1 to 4, while deposition on the levee toe increases. For instance, levee deposition at location 2 is initially at the levee crest near the channel margin (plot 2A in Figure 12), but later flood waves deposit more sediment on the lee side of the levee while sedimentation near the channel is reduced (compare plots 2B and 2C in Figure 12). The levee crest at location 1 is subaerial through most of the fourth flood wave. This forms a bed shear stress shadow and low flow velocity zone on the lee side of the levee and leads to more deposition at the levee toe than at the crest. Interestingly, deposition also increases on the up-valley side of all three levee deposits. The combination of these two depositional trends effectively increases levee length.

The transition from crest to toe deposition occurs because as the levee grows it obstructs flow and sediment transport over the crest. The transition from front-loading to back-loading can also be seen in the depositional rates measured at the crest, a down-valley position, and an up-valley position (Figure 13). For all four examples, deposition rates at the levee crest are the greatest, relative to the other locations, during the first two flood events but decrease through time (Figure 13, plotted in blue). Up-valley and down-valley depositional rates remain relatively constant at all four levee deposits

through time. Down-valley depositional rates generally exceed up-valley depositional rates (Figure 13, plotted in red), indicating levee growth is occurring in a down-valley direction. In all cases, the crest deposition rate is equal to or less than the other positions by the fourth flood wave, indicating the transition from front-loading to back-loading [*Filgueira-Rivera et al.*, 2007].

Additionally, the arrival time of the floodwave also can influence where and how levees grow. At location 4 the channel is oriented parallel to the floodplain centerline and levees should be built by classic mechanisms of turbulent eddy diffusion [*Pizzuto*, 1987; *Adams et al.*, 2004]. This assumption arises because at peak flood, floodplain flow and channelized flow should be aligned. But this site illustrates how difficult it can be to detect the controls on levee formation based on this kind of reasoning alone. At location 4, the floodwave arrives on the river right side first (Figure 10A). This sets up a water surface gradient from north to south on the river left side, which creates relatively strong flow perpendicular to the channel centerline (Figure 14A). This strong flow advects sediment from the channel into the floodplain on the river left side, and at peak discharge the gradient in sediment concentration on river left side is larger than river right (Figure 14B). In this case, the levee is genetically connected to the channel, insofar that the levee sediment was advected from the channel and immediately deposited on the margin, but the floodbasin hydrology dictates floodwave arrival time and levee formation. This location illustrates that controls on levee formation can be related to channel and floodbasin conditions.

6. Discussion: What controls levee size and shape?

It is surprising to us that there are no convincing empirical data or theory on what controls levee size and shape. Because of this we started with the null hypothesis that the levee is genetically related to the adjacent channel. Afterall, the channel is the likely source of levee sediment and the common practice of viewing levees through channel perpendicular cross-sections implies a connection. If levees were

genetically related to the adjacent channel, we would expect our data to show some relationship between levee size and local curvature, radii of curvature, or relative angle. But this is not the case: there is no interpretable relationship between river planform and the associated levee (Figures 6-9). This is surprising because if levees form as sediment diffuses and advects from the channel to the margin [*Adams et al.*, 2004], then advection should be enhanced where curvature is high because centripetal acceleration causes overbank flow, and advection should be enhanced in the crossover region because downstream oriented floodwaters would move sediment to the channel margin [*Sellin et al.*, 1993]. Even in the case of levee 4, where levee sediment is advected from the channel to the margin (Figure 14), the advection is caused by differences in floodplain arrival time, which in turn is related to inundation dynamics of the floodbasin.

Modeling results suggest levee initiation is genetically connected to the channel because levees initially form where curvature is high and shear stress is low (Figure 10B; 11). However, this genetic connection is obscured as levees grow because their inundation dynamics change. Smaller levees are inundated from crest-to-toe as floodwaters spill out of the channel and flow down the levee. But taller levees flood waters flow around the levee perimeter and inundate the levee toe first. These taller levees can exhibit a toe-to-crest inundation pattern.

This change in inundation pattern marks a significant transition in deposition. Deposition rate on smaller levees is highest on the crest because that inundates first with sediment-laden water directly from the adjacent channel (Figure 13). But deposition rate on taller levees is highest at the toe because it is inundated longest with sediment-laden floodwater. This depositional transition reshapes the levee as the toe grows faster than the crest [*Filgueira-Rivera et al.*, 2007]. The transition effectively starves the levee crest of new sediment and depending on the hydrodynamic conditions this shifts the center of mass of a levee deposit. This shift moves the levee further from the channel margin and generates levee shapes that are not easily related to the adjacent channel and its orientation.

This depositional transition results in levee progradation down-valley. Once levees are tall enough, they obstruct the propagating flood wave. The flow obstruction creates a shear stress shadow on the downstream side, and sediment transported down-valley by floodplain flow is deposited within this zone of reduced flow competence (Figure 15A). Though it is difficult to say conclusively, we propose that down-valley prograding levees explain some of the enigmatic levee topography along the Muscatatuck River (Figure 15B,C) and also make it difficult to connect the levee morphology to the adjacent channel (Figures 6-9). The modeled feedbacks between levee evolution and fluid flow suggest that after the initial levee deposition, levee morphology within fine-grained fluvial environments may be more strongly related to flood wave propagation.

We propose that the lack of relationship between the channel planform and levee size, as observed in this study, may be characteristic of fine-grained river systems. In coarser-grained rivers, the suspended sediment quickly falls out of suspension as fluid moves from the channel to the channel margin. If this is the only source of levee sediment, then the levees will be genetically connected to the channel. Indeed, consistent with this notion, *Hudson and Heitmuller* [2003] found that coarser grained levees (84^{th} percentile of grain size ranges from 64 to 240 μm) on the coastal gulf plain rivers of Mexico are largest on the outside of meander bends. This situation may not occur on finer-grained rivers. The levees and floodplain of the Muscatatuck River have much finer sediment (84^{th} percentile is 19-22 μm) with almost no sand-sized sediment (Figure 2B). We see no observable connection between the levee and adjacent river channel, possibly because as the modeling shows, fine-grained suspended sediment is transported long distances during flood before it is deposited. This can decouple the levee from the adjacent channel.

7. Conclusions

Here we tested whether levees grow and form by the transfer and deposition of sediment from the adjacent channel to the margin or by inundation dynamics in the floodbasin. If levees are formed by

sediment transfer from the adjacent channel then levee size and shape should be a function of the processes that drive that transfer. Our empirical analyses show no conclusive evidence that levee presence or size is genetically related to the planform morphology of the adjacent channel. We focused on planform attributes, like the curvature of the channel and its orientation relative to the floodplain axis, because, all else being equal, a sinuous channel should transfer more sediment to the channel margins during flood.

To see why levees may not be genetically related to their adjacent channel we conducted modeling experiments of a simplified Muscatatuck River that retains the channel planform but has a smooth floodplain. Our modeling results suggest that in fine-grained systems levee initiation is related to the channel planform. But, after levees grow tall enough relative to the floodwave, their crests are starved of sediment and the deposition maximum moves to the levee toe. When this transition occurs, levees prograde down-valley, which in turn reshapes the levee and genetically disconnects it from the channel.

From these empirical and modeling results we conclude that in fine-grained rivers, levee size and shape is sensitive to floodbasin hydrology and emerges from the interactions among inundation frequency, flood-wave propagation, and transport pathways of suspended sediment.

Acknowledgements

We would like to think the donors of the American Chemical Society Petroleum Research Fund for supporting this work. We would also like to thank the Indiana University Grand Challenges *Preparing for Environmental Change* for partial support. GJ would like to thank the American Association of Petroleum Geologists and the Society for Sedimentary Geology for providing additional research grants in support of field and laboratory work. Upon publication all data will be made available through Indiana University's Scholar Works (https://scholarworks.iu.edu/).

480

481 **Table 1**.

Table 1 Summarized model parameters for Delft3D		
Hydrodynamic Parameters		
Water Density	1000	kg/m^3
Horizontal Eddy Viscosity	0.001	m^2/s
Horizontal Eddy Diffusivity	1	m^2/s
3D Turbulence Model[a]	κ-ϵ	--
Manning Roughness	0.035	--
Sediment Parameters		
Settling Velocity	0.23	mm/s
Specific Density	2650	kg/m^3
Dry Bed Density	1350	kg/m^3
Density for Hindered Settling	1600	kg/m^3
τ-crit for Sedimentation[b]	0.5	N/m^2
τ-crit for Erosion[c]	2	N/m^2
Erosion Parameter	0.0001	$kg/m^2/s$
Initial Sediment Layer	0.5	m
Morphological Scaling Factor	70	--

482

483 [a] Kappa-Epsilon (κ-ϵ) 3-dimensional turbulence closure model

484 [b] Critical shear stress for sedimentation

485 [c] Critical shear stress for erosion

486

487 **Table 2:** Levee statistics on Reaches 1 and 2 of the Muscatatuck River

	Median Height (m)	Range in levee height (m)	Median width (m)	Range in levee Width (m)
Reach 1 – river left	0.21	0.05 – 0.84	16.9	0.6 – 30.7
Reach 1 – river right	0.19	0.08 – 1.1	13.8	0.6 – 36.2
Reach 2 – river left	0.20	0.04 - 0.9	21.9	4.2 – 16.1
Reach 2– river right	0.17	0.07 - 0.7	16.1	6.3 – 38.8

488

Figures and Captions

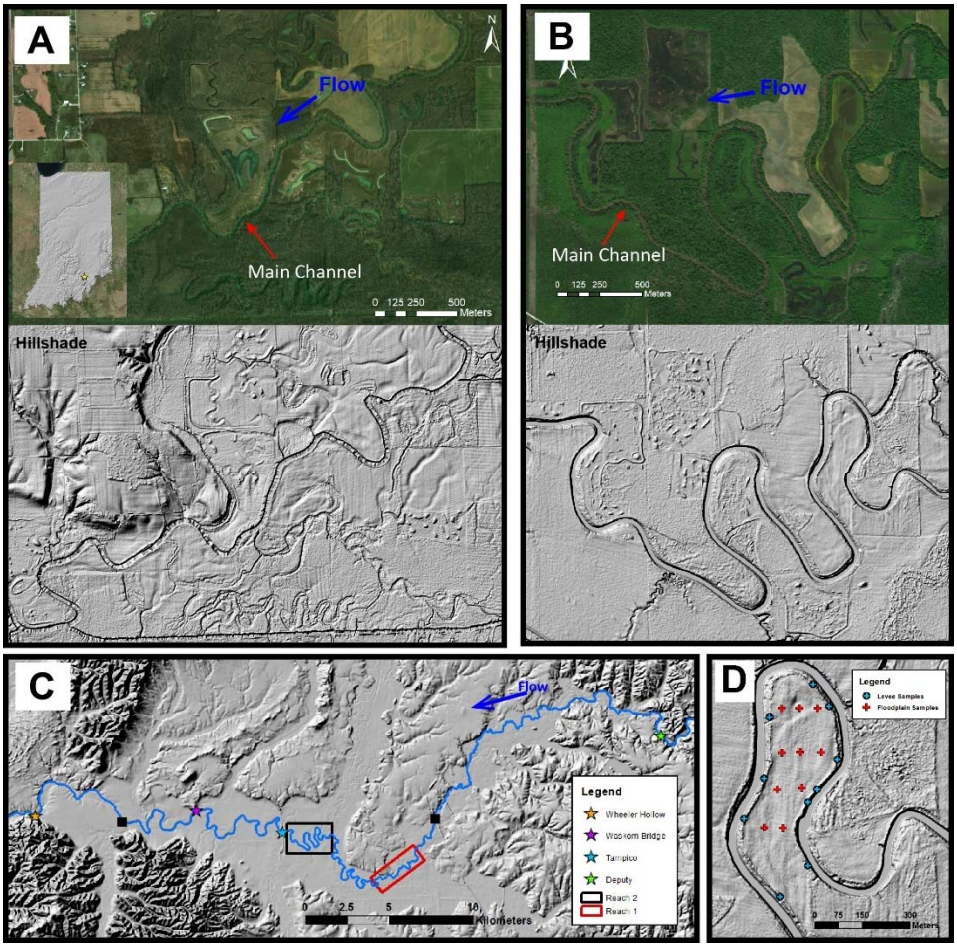

Figure 1. (A, B) Satellite and a hillshade image, generated from 1.5-meter resolution elevation data, for Reaches 1 and 2 along the Muscatatuck River, Indiana. Flow direction in the main channel is indicated on the satellite imagery. Channel bathymetry is from hydro-flattening. (C) Longer reach showing the locations of Reaches 1 and 2 (boxes), and locations of river-spanning bridges where suspended sediment samples were collected (stars). These are also locations of USGS gauges used for data in figures 2. Black squares mark the beginning and end of the reach of the Muscatatuck River analyzed in radius of curvature analysis in figure 6. (D) Sediment sample locations along Reach 2. Inset map in (A) shows location of study reaches in Indiana.

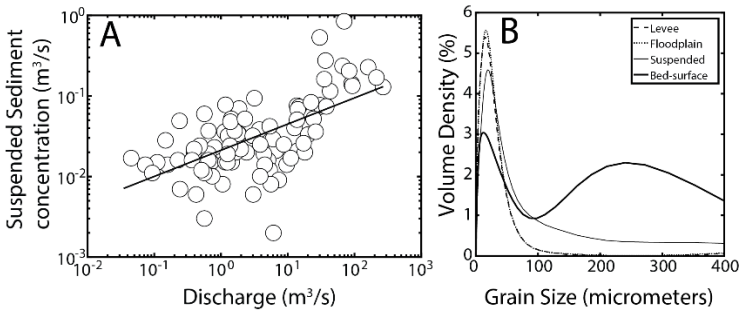

Figure 2. (A) Suspended sediment rating curve for the Muscatatuck River from USGS suspended sediment concentration samples collected at the Deputy, Indiana gauge station. (B) Channel-bed-surface distribution is the average of four samples collected near Waskom and Wheeler Hollow bridges and suspended sediment distribution is the average of 51 samples collected at Deputy and Wheeler Hollow. Floodplain and levee crest grain size distributions are the averages of ten samples collected along Reach 2. In all cases, sample locations are shown in Figure 1C.

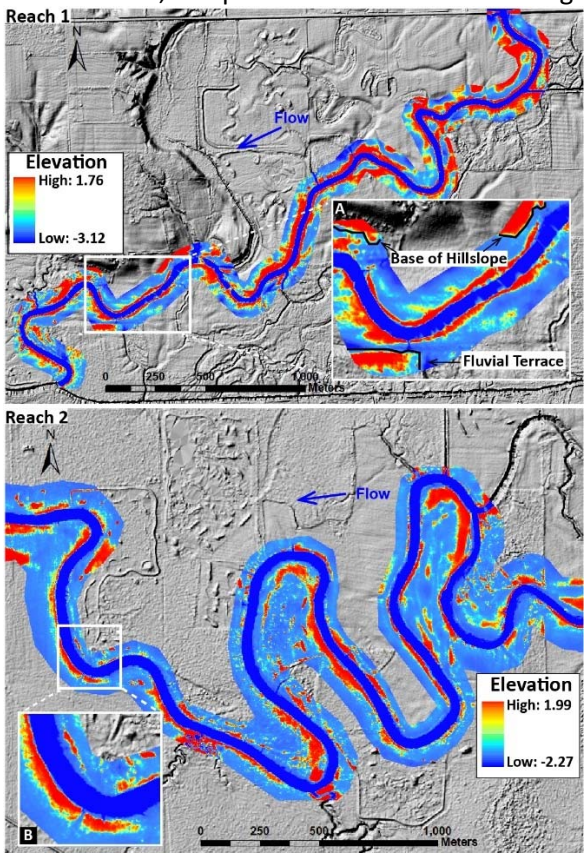

Figure 3. Histogram equalization and detrending visualization methods for near-channel topography along Reach 1 and Reach 2 of the Muscatatuck River. Elevation is measured relative to the detrended floodplain surface.

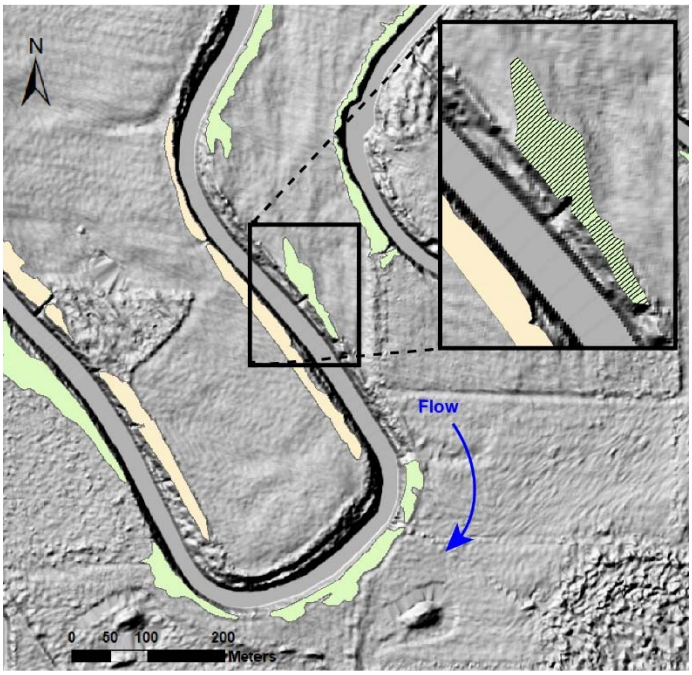

Figure 4. Examples of closed-contour polygons showing the spatial extent of the levee deposits determined from levee toe contour elevation. The levee widths and height values were extracted for each levee polygon. Levee width is measure along channel-perpendicular transects clipped to the levee polygon extent, as shown in inset box. Colors indicate river right or river left side.

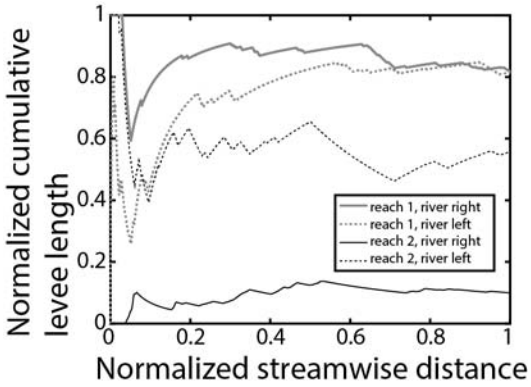

Figure 5. Levee presence along Reaches 1 and 2. Levee length is measured cumulatively and nondimensionalized by cumulative bank length. Increases and decreases in normalized levee length, respectively, represent leveed and unleveed parts of the reach.

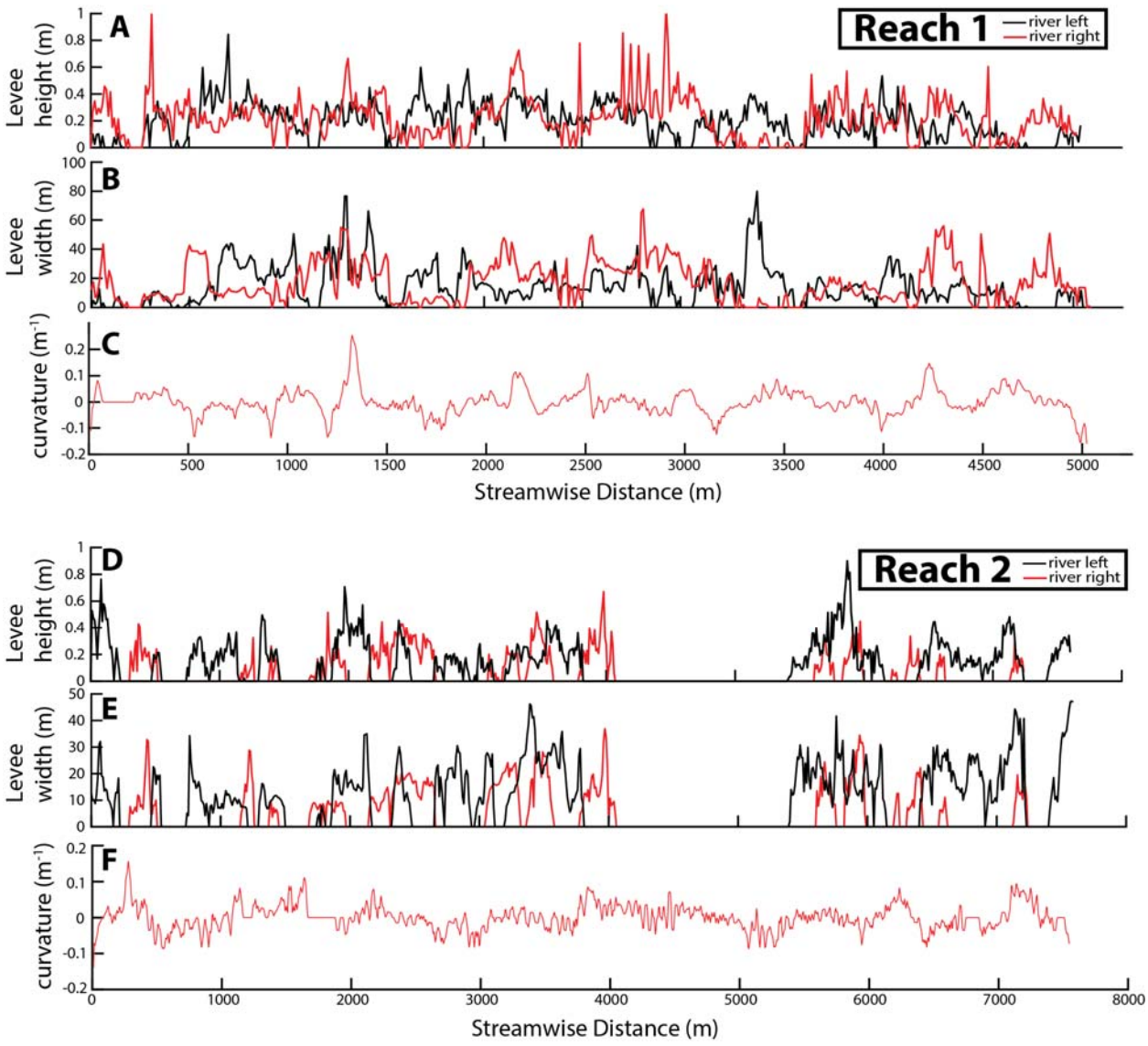

Figure 6. For both reaches, levee height (A, D) and width (B, E) are shown for every 2-meter channel-perpendicular cross-section. (see example in Figure 4). Curvature (C, F) is calculated from the channel centerline following Schwenk et al., (2017).

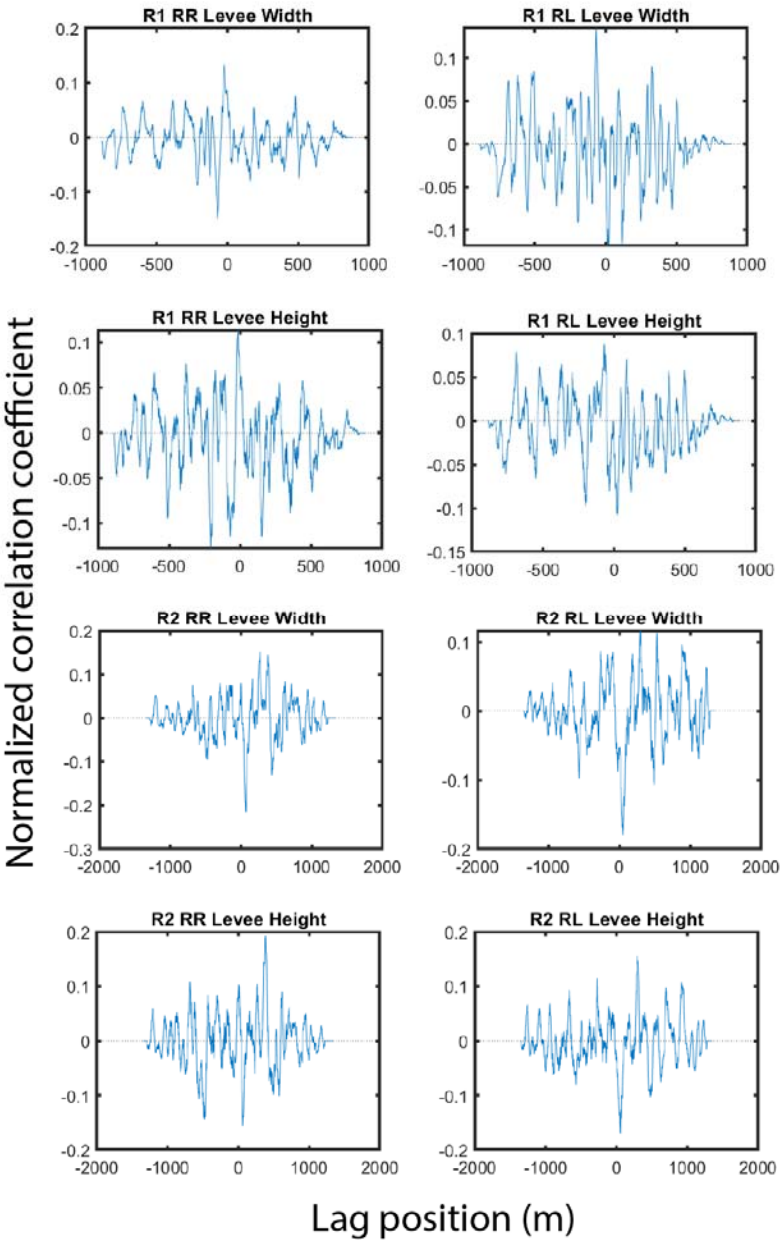

Figure 7. Cross-correlation function between channel curvature and levee height and width data at different lag positions. R1 – Reach 1; R2 – Reach 2; RR – River Right; RL – River Left.

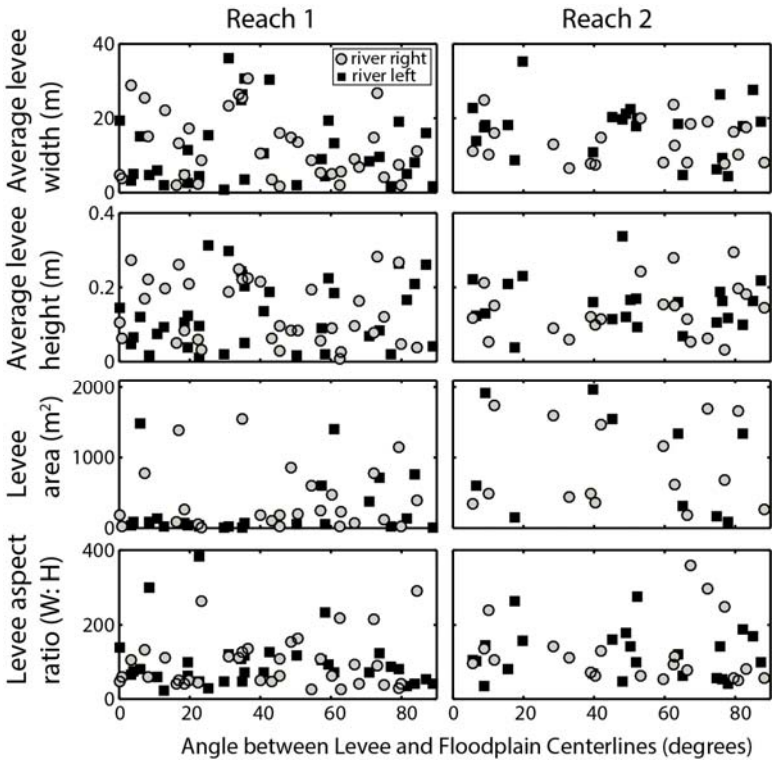

Figure 8. Levee morphometrics plotted against relative orientation for Reaches 1 and 2 along the Muscatatuck River. Relative orientation (in degrees) is the angle between the centerline of the levee and floodplain. Zero indicates the long-axis of the levee is parallel to the floodplain centerline. Data are average values for each closed-contour levee polygon (see example in Figure 4). See Figure 1 A,B for location of these reaches.

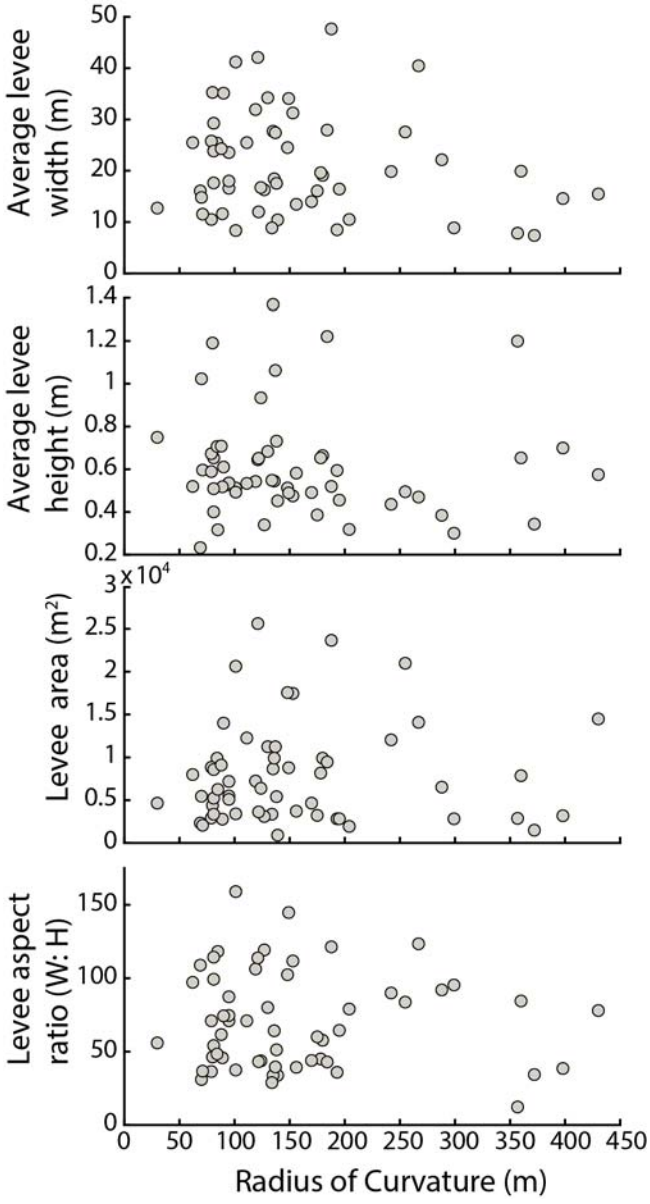

Figure 9. Levee morphometrics plotted against channel radius of curvature for 54 meander bends along the Muscatatuck River. See Figure 1C for location of this reach.

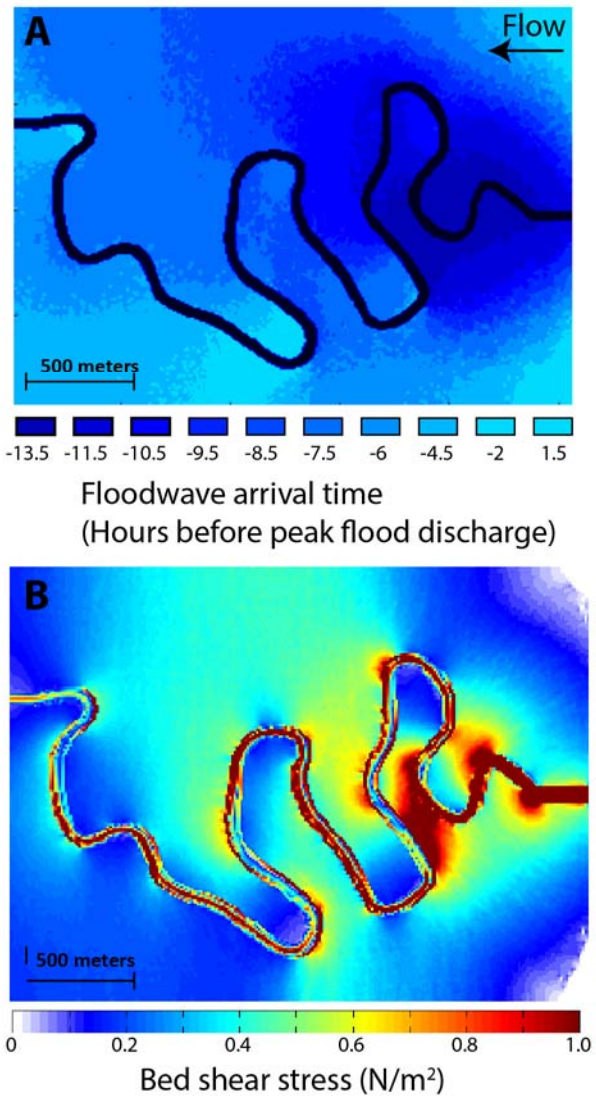

542

543 Figure 10: (A) Map of floodwave arrival time prior to any morphodynamic change. Floodwave arrival is
544 defined as inundation greater than 10 cm. The inundation front is noisy because of the random
545 topographic roughness. Negative numbers indicate floodwave arrival before peak flood. (B) Bed shear
546 stress at peak discharge prior to any morphodynamic change.

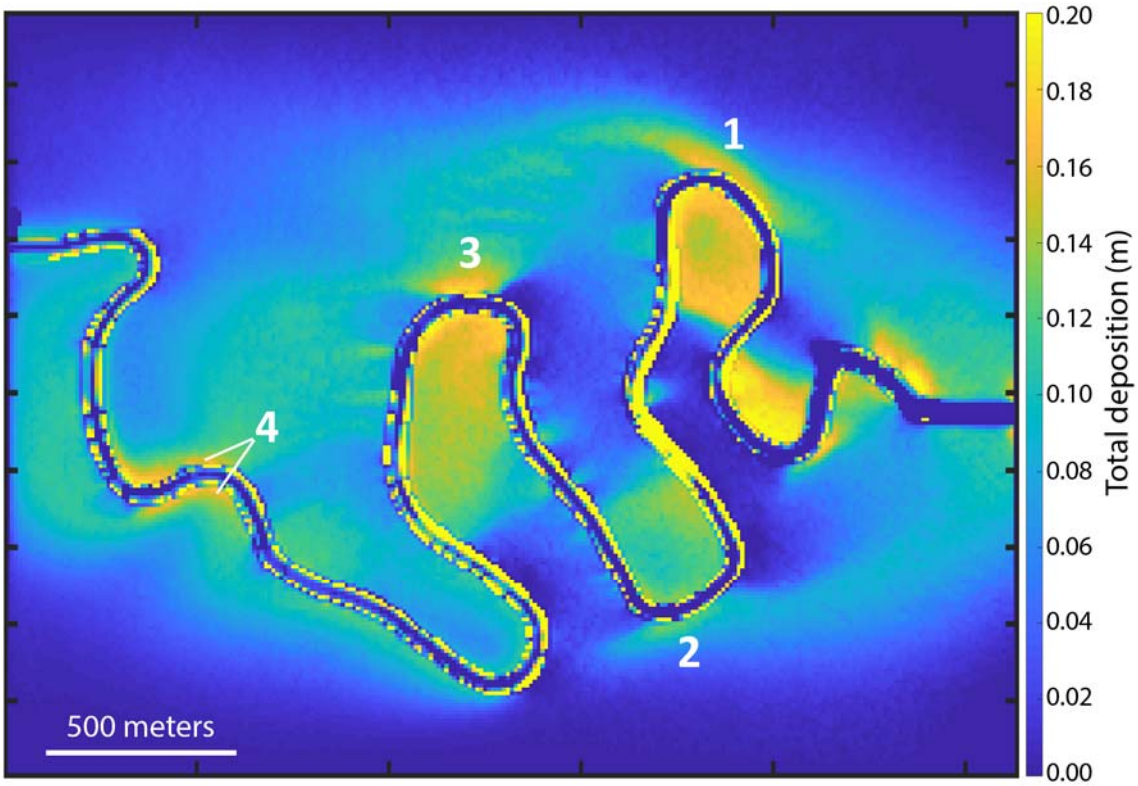

547

548 **Figure 11:** Total deposition in the model domain over the four flood-wave experiment. Numbers 1-4
549 refer to levees analyzed in Figures 12-14.

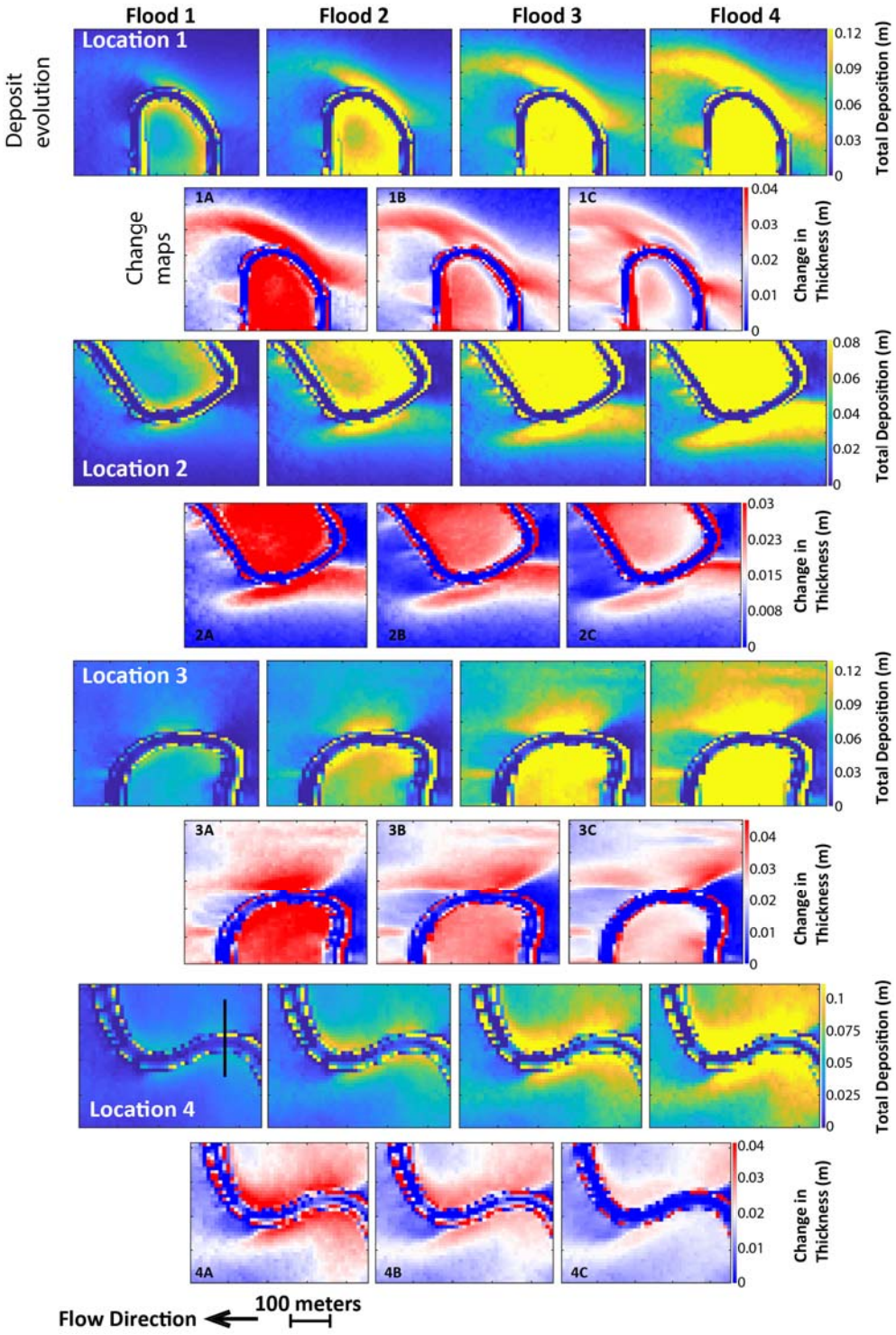

Figure 12: Time evolution of levee thicknesses for locations 1-4. For each levee, the top row shows development of the total deposit after each floodwave is complete, and bottom row shows the change between each flood.

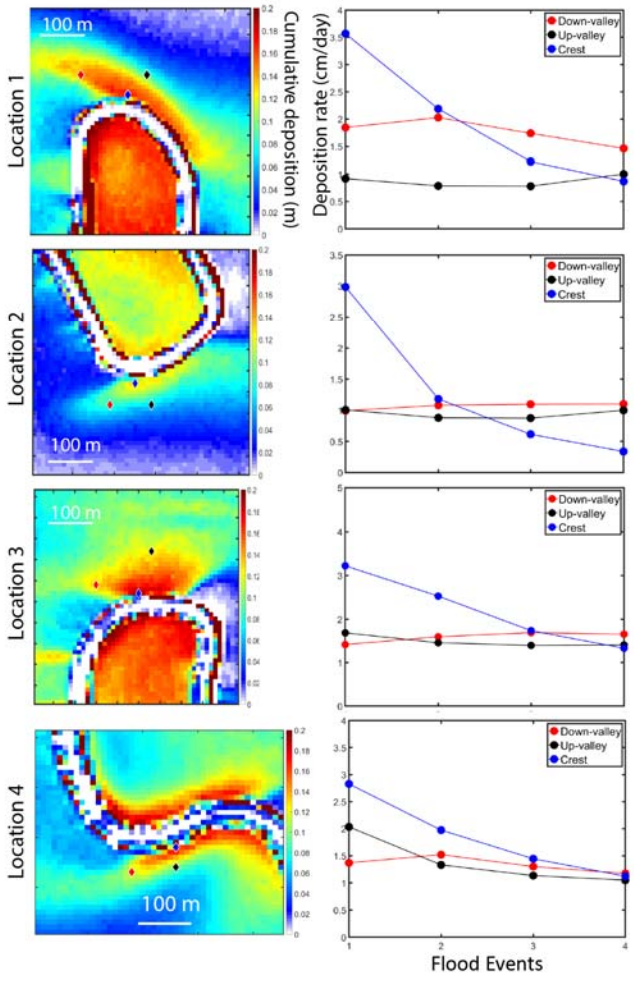

554

555 Figure 13: Deposition rate on the levee crest decreases with time and all levees show a transition, by the
556 fourth flood wave, where the highest deposition rate is on the levee toe.

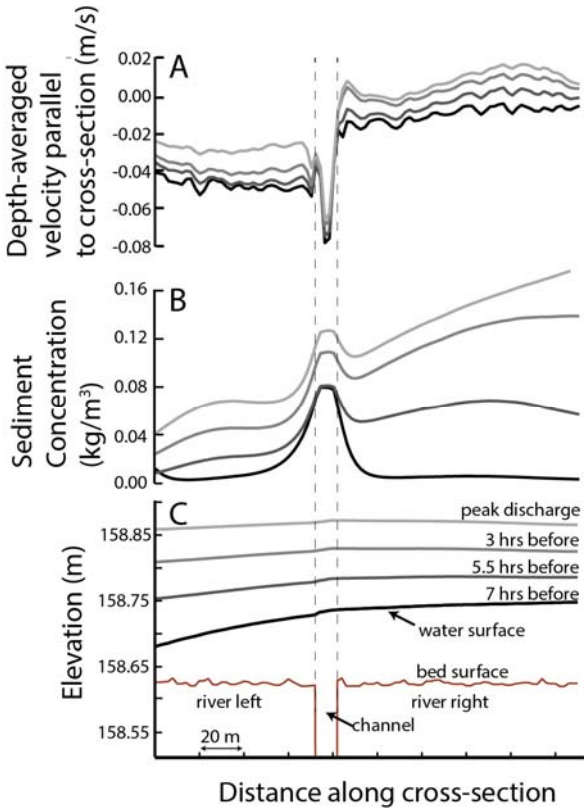

Figure 14: Time evolution of cross-section parallel flow velocity (A), sediment concentration (B), and water surface (C) at location 4 during flood 1. Flow is into the page, and negative velocities in C correspond to a southerly flow direction, while positive velocities mean northerly flow. Cross-section location is shown on the first panel for location 4 on Figure 12.

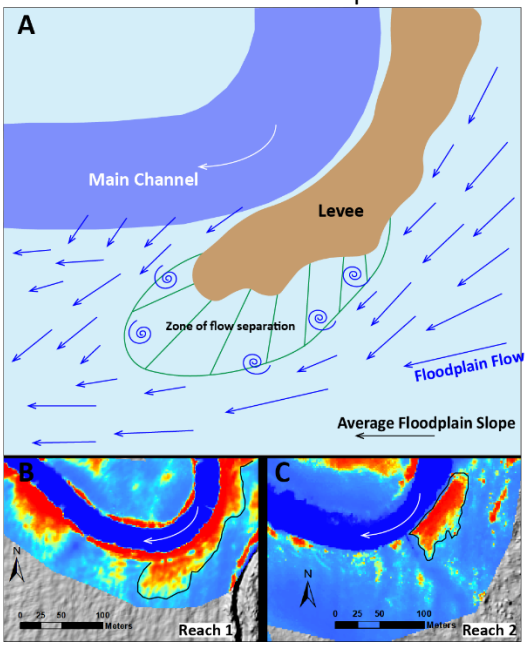

Figure 15: A) Cartoon showing how tall levees create flow shadows and deposition leading to down-valley progradation. B,C) Possible examples of progradational levee morphologies on Reaches 1 and 2.

References

Adams, P. N., R. L. Slingerland, and N. D. Smith (2004), Variations in natural levee morphology in anastomosed channel flood plain complexes, *Geomorphology*, *61*(1-2), 127-142.

Asselman, N. E. M., and H. Middelkoop (1995), FLOODPLAIN SEDIMENTATION - QUANTITIES, PATTERNS AND PROCESSES, *Earth Surface Processes and Landforms*, *20*(6), 481-499, doi:10.1002/esp.3290200602.

Brakenridge, G., J. Syvitski, E. Niebuhr, I. Overeem, S. Higgins, A. Kettner, and L. Prades (2017), Design with nature: Causation and avoidance of catastrophic flooding, Myanmar, *Earth-science reviews*, *165*, 81-109.

Brierley, G. J., R. J. Ferguson, and K. J. Woolfe (1997), What is a fluvial levee?, *Sedimentary Geology*, *114*(1-4), 1-9, doi:10.1016/s0037-0738(97)00114-0.

Brooks, G. R. (2005), Overbank deposition along the concave side of the Red River meanders, Manitoba, and its geomorphic significance, *Earth Surface Processes and Landforms*, *30*(13), 1617-1632, doi:10.1002/esp.1219.

Bryant, M., P. Falk, and C. Paola (1995), Experimental study of avulsion frequency and rate of deposition, *Geology*, *23(4)*, 365-368.

Cazanacli, D., and N. D. Smith (1998), A study of morphology and texture of natural levees—Cumberland Marshes, Saskatchewan, Canada, *Geomorphology*, *25*(1-2), 43-55.

Clark, L., and T. Wynn (2007), Methods for determining streambank critical shear stress and soil erodibility: implications for erosion rate predictions, *Transactions of the ASABE*, *50*(1), 95-106.

Czuba, J., S. R. David, D. A. Edmonds, and A. S. Ward (accepted), Dynamics of surface-water connectivity in a low-gradient meandering river floodplain, *Water Resources Research*, doi.org/10.1029/2018WR023527

David, S. R., D. A. Edmonds, and S. L. Letsinger (2017), Controls on the occurrence and prevalence of floodplain channels in meandering rivers, *Earth Surface Processes and Landforms*, n/a-n/a, doi:10.1002/esp.4002.

Edwards, T. K., G. D. Glysson, H. P. Guy, and V. W. Norman (1999), *Field methods for measurement of fluvial sediment*, US Geological Survey Denver, CO.

Ervine, D. A., K. Babaeyan-Koopaei, and R. H. Sellin (2000), Two-dimensional solution for straight and meandering overbank flows, *Journal of Hydraulic Engineering*, *126*(9), 653-669.

Ervine, D. A., B. B. Willetts, R. H. J. Sellin, and M. Lorena (1993), Factors affecting conveyance in meandering compound flows, *Journal of Hydraulic Engineering*, *119*(12), 1383-1399.

Ferguson, R., and M. Church (2004), A simple universal equation for grain settling velocity, *Journal of Sedimentary Research*, *74*(6), 933-937.

Ferguson, R. J., and G. J. Brierley (1999), Levee Morphology and Sedimentology Along the Lower Tuross River, South-Eastern Australia, *Sedimentology*, *46*, 627-648.

Fielding, C. R., and R. C. Crane (1987), An application of statistical modelling to the prediction of hydrocarbon recovery factors in fluvial reservoir sequences.

Filgueira-Rivera, M., N. D. Smith, and R. L. Slingerland (2007), Controls on natural levee development in the Columbia River, British Columbia, Canada, *Sedimentology*, *54*(4), 905-919.

Hudson, P. F., and F. T. Heitmuller (2003), Local- and watershed-scale controls on the spatial variability of natural levee deposits in a large fine-grained floodplain: Lower Panuco Basin, Mexico, *Geomorphology*, *56*(3-4), 255-269, doi:10.1016/s0169-555x(03)00155-7.

Hum, Y. C., K. W. Lai, and M. I. Mohamad Salim (2014), Multiobjectives bihistogram equalization for image contrast enhancement, *Complexity*, *20*(2), 22-36.

Iseya, F., and H. Ikeda (1989), *Sedimentation in coarse-grained sand-bedded meanders: distinctive deposition of suspended sediment*, Terra Scientific Publishing (TERRAPUB): Tokyo.

James, C. S. (1985), SEDIMENT TRANSFER TO OVERBANK SECTIONS, *Journal of Hydraulic Research*, *23*(5), 435-452.

Kesel, R. H., K. C. Dunne, R. C. McDonald, K. R. Allison, and B. E. Spicer (1974), Lateral erosion and overbank deposition on the Mississippi River in Louisiana caused by 1973 flooding, *Geology*, *1*, 461-464.

Kimiaghalam, N., S. P. Clark, and H. Ahmari (2016), An experimental study on the effects of physical, mechanical, and electrochemical properties of natural cohesive soils on critical shear stress and erosion rate, *International Journal of Sediment Research*, *31*(1), 1-15.

Mackey, S. D., and J. S. Bridge (1995), Three-dimensional model of alluvial stratigraphy: Theory and application, *Journal of Sedimentary Research*, *B65*, 7-31.

Marriott, S. (1992), Textural analysis and modelling of a flood deposit: River Severn, U.K., *Earth Surface Process and Landforms*, *17*, 687-697.

Mertes, L. A. K. (1997), Documentation and significance of the perirheic zone on inundated floodplains, *Water Resources Research*, *33*(7), 1749-1762.

Middelkoop, H., and M. Van der Perk (1998), Modelling spatial patterns of overbank sedimentation on embanked floodplains, *Geografiska Annaler Series a-Physical Geography*, *80A*(2), 95-109, doi:10.1111/j.0435-3676.1998.00029.x.

Mohrig, D., P. L. Heller, C. Paola, and W. J. Lyons (2000), Interpreting avulsion process from ancient alluvial sequences: Guadalope-Matarranya system (northern Spain) and Wasatch Formation (western Colorado), *Geological Society of America Bulletin*, *112*(12), 1787.

661 Nanson, G., and J. Croke (1992), A genetic classification of floodplains, *Geomorphology*, *4*(6), 459-486.
662
663 Nezu, I., and H. Nakagawa (1993), *Turbulence in Open-Channel Flows*, 281 pp., A.A. Balkema, Rotterdam
664 Brookfield.
665
666 Nicholas, A. P., and C. A. Mitchell (2003), Numerical simulation of overbank processes in topographically
667 complex floodplain environments, *Hydrological Processes*, *17*(4), 727-746, doi:10.1002/hyp.1162.
668
669 Pierik, H., E. Stouthamer, and K. Cohen (2017), Natural levee evolution in the Rhine-Meuse delta, the
670 Netherlands, during the first millennium CE, *Geomorphology*, *295*, 215-234.
671
672 Pizzuto, J. E. (1987), Sediment diffusion during overbank flows, *Sedimentology*, *34*, 301-317.
673
674 Pizzuto, J. E., J. A. Moody, and R. H. Meade (2008), Anatomy and dynamics of a floodplain, Powder River,
675 Montana, USA, *Journal of Sedimentary Research*, *78*(1), 16-28.
676
677 Schwenk, J., A. Khandelwal, M. Fratkin, V. Kumar, and E. Foufoula-Georgiou (2017), High spatiotemporal
678 resolution of river planform dynamics from Landsat: The RivMAP toolbox and results from the
679 Ucayali
680 River, *Earth and Space Science*, *4*(2), 46-75.
681
682 Sellin, R. H. J., D. A. Ervine, and B. B. Willetts (1993), Behavoir of meandering two-stage channels, *Proc.*
683 *Instn. Civ. Engrs. Wat., Marit. & Energy*, *101*, 99-111.
684
685 Shiono, K., and D. W. Knight (1991), Turbulent open-channel flows with variable depth across the
686 channel, *Journal of Fluid Mechanics*, *222*, 617-646.
687
688 Shiono, K., and Y. Muto (1998), Complex flow mechanisms in compound meandering channels with
689 overbank flow, edited, Cambridge University Press.
690
691 Smith, N. D., T. A. Cross, J. P. Dufficy, and S. R. Clough (1989), Anatomy of an avulsion, *Sedimentology*,
692 *36*, 1-23.
693
694 Walling, D., and Q. He (1998), The spatial variability of overbank sedimentation on river floodplains,
695 *Geomorphology*, *24*(2), 209-223.
696
697 Wolfert, H., P. Hommel, A. Prins, and M. Stam (2002), The formation of natural levees as a disturbance
698 process significant to the conservation of riverine pastures, *Landscape ecology*, *17*(1), 47-57.
699
700